Post-Error Correction for Quantum Annealing Processor using Reinforcement Learning

Tomasz Śmierzchalski[1,2], Łukasz Pawela[2], Zbigniew Puchała[2,3], Tomasz Trzcinski[1], and Bartłomiej Gardas[2]

[1] Warsaw University of Technology, Pl. Politechniki 1, 00-661 Warsaw, Poland
[2] Institute of Theoretical and Applied Informatics, Polish Academy of Sciences, Bałtycka 5, 44-100 Gliwice, Poland
[3] Faculty of Physics, Astronomy and Applied Computer Science, Jagiellonian University, 30-348 Kraków, Poland

Abstract. Finding the ground state of the Ising spin-glass is an important and challenging problem (NP-hard, in fact) in condensed matter physics. However, its applications spread far beyond physic due to its deep relation to various combinatorial optimization problems, such as travelling salesman or protein folding. Sophisticated and promising new methods for solving Ising instances rely on quantum resources. In particular, quantum annealing is a quantum computation paradigm, that is especially well suited for Quadratic Unconstrained Binary Optimization (QUBO). Nevertheless, commercially available quantum annealers (i.e., D-Wave) are prone to various errors, and their ability to find low energetic states (corresponding to solutions of superior quality) is limited. This naturally calls for a post-processing procedure to correct errors (capable of lowering the energy found by the annealer). As a proof-of-concept, this work combines the recent ideas revolving around the DIRAC architecture with the Chimera topology and applies them in a real-world setting as an error-correcting scheme for quantum annealers. Our preliminary results show how to correct states output by quantum annealers using reinforcement learning. Such an approach exhibits excellent scalability, as it can be trained on small instances and deployed for large ones. However, its performance on the chimera graph is still inferior to a typical algorithm one could incorporate in this context, e.g., simulated annealing.

Keywords: Quantum error correction · Quantum Annealing · Deep reinforcement learning · Graph neural networks.

1 Introduction

Many complex and significant optimization problems (such as all of Karp's 21 NP-complete problems [18], the travelling salesman problem [17], the protein folding problem [3], financial portfolio management [26]) can be mapped into the problem of finding the ground state of the Ising spin-glass. Sophisticated and

promising new methods for solving Ising instances rely on quantum computation, particularly quantum annealing.

Quantum annealing is a form of quantum computing particularly well-tailored for optimization [13,27]. It is closely related to adiabatic quantum computation [19], a paradigm of universal quantum computation which relies on the adiabatic theorem [14] to perform calculations. It is equivalent (up to polynomial overhead) to the better-known gate model of quantum computation [19]. Nevertheless, commercially available quantum annealers (i.e., D-Wave) are prone to various errors, and their ability to find low energetic states is limited.

Inspired by the recently proposed deep reinforcement learning method for finding spin glass ground states [8], here, we propose a new post-processing error correction schema for quantum annealers called Simulated Annealing with Reinforcement (SAwR). In this procedure, we combine deep reinforcement learning with simulated annealing. We employ a graph neural network to encode the Ising instance into an ensemble of low-dimensional vectors used for reinforcement learning. The agent learns a strategy for improving (finding a lower energy state) solutions given by the physical quantum annealer. The process of finding the lower energy state involves "flipping" spins one by one according to the learned strategy and recording the energy state after each step. The solution is defined as the lowest energy state found during this procedure. In Simulated Annealing with Reinforcement, we start with simulated annealing and, at low temperature, we replace the Metropolis-Hasting criterion with a single pass of spin flipping procedure.

Unlike recent error-correcting schema [24,25,30] we do not utilize multiple physical qubits for representing single logical qubits. This approach allows for a far greater size of problems to which our method applies. However, the performance of SAwR is still inferior to a typical algorithm one could incorporate in this context, such as simulated annealing. Nevertheless, using reinforcement learning for post-error correction is still an open and promising avenue of research.

2 Ising Spin Glass and Quantum Annealing

2.1 Quantum Annealing in D-Wave

The Ising problem is defined on some arbitrary simple graph G. An Ising Hamiltonian is given by:

$$H_{\text{Ising}}(\sigma) = \sum_{\langle i,j \rangle \in G} J_{i,j} \sigma_i \sigma_j + \sum_i h_i \sigma_i, \tag{1}$$

where $\sigma_i \in \{+1, -1\}$ denotes the i-th Ising spin, $\sigma = \{\sigma_1, \ldots, \sigma_n\}$ is the vector representation of a spin configuration. $\langle i,j \rangle$ denotes neighbours in graph G, $J_{i,j}$ strength of interaction (coupling coefficient) between i-th and j-th spin.
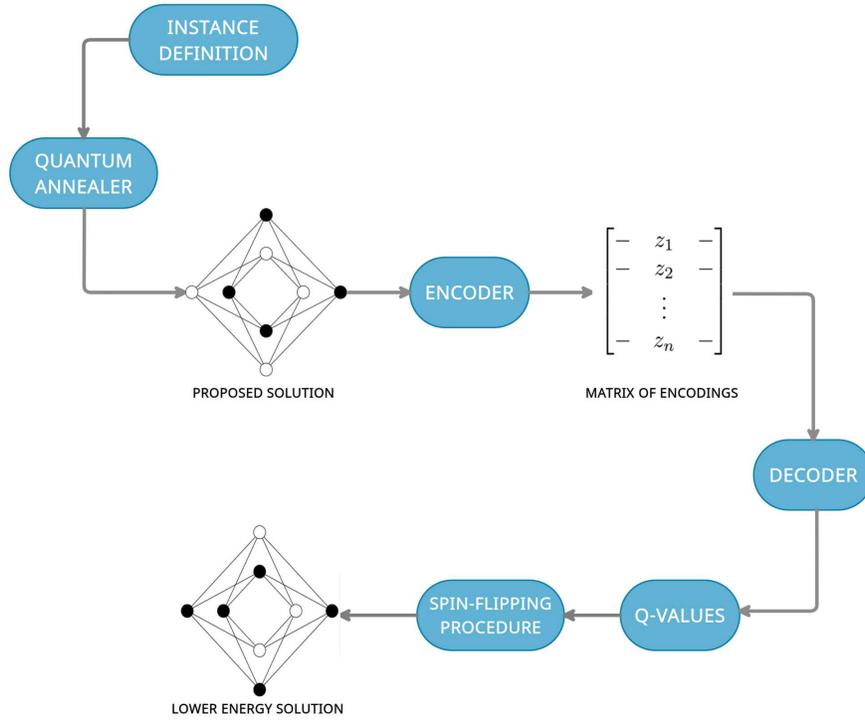
Fig. 1: Overview of our method, arrows represent subsequent steps. First, we define the Ising instance by providing couplings strength and biases (external magnetic field strength). Then we obtain the proposed solution from a quantum annealer. Here, it is represented by a single Chimera unit cell rendered as a graph. Black nodes represent spin value $\sigma_i = -1$ and white nodes represent spin value $\sigma_i = 1$. Edges represent couplings between spins. In the next step, we encode such an instance using a graph neural network into the matrix of encodings, where each row corresponds to the embedding of a vertex. Then this matrix is passed through a decoder to obtain Q-values of actions associated with each vertex. The spin flipping procedure involves "flipping" spins one by one according to Q-Values, starting from the highest and recording the energy state after each step. The solution is defined as the lowest energy state found during this procedure.

h_i is external magnetic field (bias) affecting i-th spin. The goal is to find spin configuration, called ground state,

$$\sigma^* = \arg\min_{\sigma} H_{\text{Ising}}(\sigma). \tag{2}$$

such that energy of H_{Ising} is minimal. This is an NP-hard problem. Quantum annealing is a method for finding the ground state of (1). This is done by adiabatic

evolution from the initial Hamiltonian H_X of the Transverse-field Ising model to the final Hamiltonian H_{Ising}. The Hamiltonian of this process is described by

$$\mathcal{H}(t) = A(t)H_X + B(t)H_{\text{Ising}}, \tag{3}$$

where $H_X = \sum_i \hat{\sigma_i}^x$ and $\hat{\sigma_i}^x$ is the standard Pauli X matrix acting on the i-th qubit. The function $A(t)$ decreases monotonically to zero, while $B(t)$ increases monotonically from zero, with $t \in [0, t_f]$, where t_f denotes total time of anneal [11,27]. For a closed system, the adiabatic theorem guarantees that if the initial state is the ground state, then the final state will be arbitrarily close to the ground state, provided all technical requirements are met [14]. In summary, the systems start with a set of qubits, each in a superposition state of -1 and 1. By annealing, the system collapses into the classical state that represents the minimum energy state of the problem, or one very close to it.

The D-Wave 2000Q is a psychical realization of the quantum annealing algorithm. Sadly, the idealized conditions of the adiabatic theorem are nearly impossible to be realized in a physical device. In such an open system, there is inevitable thermal noise which may cause decoherence [7]. Furthermore, due to technical limitations, those device suffers from programming control errors on the h_i and $J_{i,j}$ terms, which can unintentionally cause the annealer to evolve according to the wrong Hamiltonian [1].

2.2   D-Wave 2000Q

At the heart of every D-wave quantum annealer lies the Quantum Processing Unit (QPU), which is a lattice of interconnected qubits. While its physical details are beyond the scope of this paper[4], it is necessary to mention some technical details. In QPU, qubits can be thought of as loops being "oriented" vertically or horizontally (see figure 2) and connected to each other via devices called couplers. How qubits and couplers are interconnected is described by QPU topology.

As of the time of writing, there are two available architectures of D-Wave quantum annealers, namely 2000Q with Chimera topology deployed in 2017 and Advantage with Pegasus topology deployed in 2020. Third, called Advantage 2 with Zephyr topology [2] is stated to release in 2023-2024 [5]. In this work, we will focus on the 2000Q device and Chimera topology.

Chimera Topology   The basic building block of Chimera topology is a set of connected qubits called a unit cell. Each unit cell consists of four horizontal qubits connected to four vertical qubits via couplers which form bipartite connectivity as seen in figure 3. Unit cells are tiled vertically and horizontally with adjacent qubits connected, creating a lattice of sparsely connected qubits.

It is conceptually valuable to categorize couplers into *internal couplers* which connect intersecting (orthogonal) qubits and *external couplers* which connect colinear pairs of qubits (that is, pairs of qubits that lie in the same row or

---

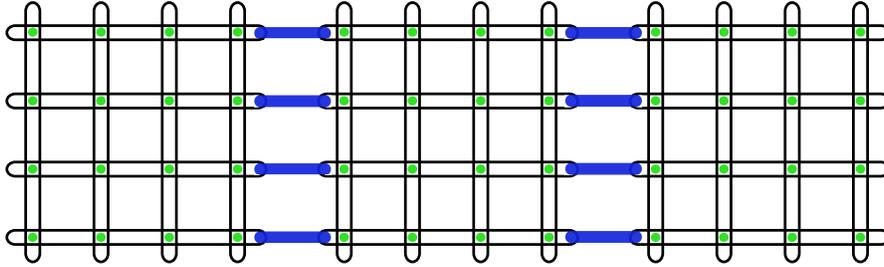[4] Interested reader may find details in [4] and [12]

Fig. 2: Qubits are represented as horizontal and vertical loops. This graphic shows three coupled unit cells with eight qubits each. Green dots represent internal couplers connecting qubits inside the unit cell, while blue bars represent external couplers connecting different unit cells.

column). The notation C_n describes the Chimera grid composed of $n \times n$ coupled unit cells, consisting of $8n^2$ qubits. D-Wave 2000Q device is equipped with C_{16} QPU, with more than 2000 qubits [6].

(a) Unit cell rendered as column

(b) Unit cell rendered as cross

Fig. 3: Different renderings of Chimera unit cell as graph. Nodes represent qubits and edges represent internal couplers.

3   Results

3.1   Reinforcement Learning Formulation

We will consider standard reinforcement learning setting defined as Markov Decision Process [29] where an agent interacts with an environment over a number of discrete time steps $t = 0, 1, \ldots, T$. At each time step t, the agent receives a state s_t and selects an action a_t from some set of possible actions $\mathcal{A}$ according to its policy π, where π is a mapping from set of states $\mathcal{S}$ to set of actions $\mathcal{A}$.
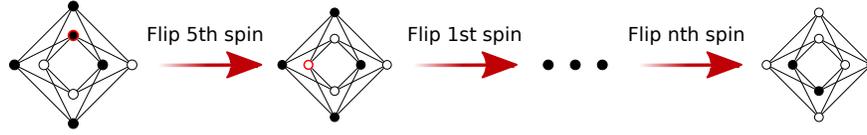
Fig. 4: Overview of single episode. To simplify, we show it on a single Chimera unit cell. White nodes represent $\sigma_i = 1$ and black nodes represent $\sigma_i = -1$ We start in some state s_0 and one by one we flip spins until all spins are flipped. The solution is defined as spin configuration σ^* corresponding lowest energy state found during this procedure.

In return, the agent receives a scalar reward r_t and moves to next state s_{t+1}. The process continues until the agent reaches a terminal state s_T after which the process restarts. We call one pass of such process an episode. The return at time step t, denoted $R_t = \sum_{k=0}^{T-t} \gamma^k r_{t+k}$ is defined as sum of rewards that agent will receive for rest of the episode discounted by discount factor $\gamma \in (0, 1]$. The goal of the agent is to maximize the expected return from each state s_t.

   We will start by defining state, action, and reward in the context of the Ising spin-glass model.

   – **State**: a state s represents the observed spin glass instance, including both the spin configuration σ, the coupling strengths $\{J_{ij}\}$ and values of external magnetic field $\{h_i\}$.
   – **Action**: an action $a^{(i)}$ means to flip spin i. By flipping spin we mean changing is value to opposite. For example, after agent performs action $a^{(i)}$, spin $\sigma_i = 1$ becomes $\sigma_i = -1$. Agent can flip each spin once.
   – **Reward**: the reward $r(s_t; a_t^{(i)}; s_{t+1})$ is defined as the energy change after flipping spin i from state s_t to a new state s_{t+1}.

   Starting at $t = 0$, an agent flips one spin during each time step, which moves him to the next state (different spin configuration). The terminal state s_T is met when the agent has flipped each spin. The solution is defined as spin configuration σ corresponding lowest energy state found during this procedure.

   An action-value function $Q^\pi(s, a) = \mathbb{E}(R_t \mid s_t = s, \ a_t = a)$ is the expected return for selecting action a in state s and following policy π. The value $Q^\pi(s, a)$ is often called Q-value of action a in state s. The optimal action-value function $Q^*(s, a) = \max_\pi Q^\pi(s, a)$ which gives the maximum action value for state s and action a achievable by any policy. As learning optimal action-value function is in practice infeasible, We seek to learn function approximator $Q(s, a; \Theta) \approx Q^*(s, a)$ where Θ is set of learnable model parameters. We denote policy used in such aproximation as π_Θ.

3.2   Model Architecture

Our model architecture is inspired by DIRAC (**D**eep reinforcement learning for sp**I**n-glass g**R**ound-st**A**te **C**alculation), an Encoder-Decoder architecture introduced in [8]. It exploits the fact that the Ising spin-glass instance is wholly

described by the underlying graph. In this view, couplings $J_{i,j}$ become edge weights, external magnetic field h_i and spin σ_i become node weights. Employing DIRAC is a two-step process. At first, it encodes the whole spin-glass instance such that every node is embedded into a low-dimensional vector, and then the decoder leverages those embeddings to calculate the Q-value of every possible action. Then, the agent chooses the action with the highest Q-value. In the next sections, We will describe those steps in detail.

Encoding As described above, the Ising spin-glass instance can be described in the language of graph theory. It allows Us to employ graph neural networks [10,9], which are neural networks designed to take graphs as inputs. We use modified SGNN (**S**pin **G**lass **N**eural **N**etwork) [8] to obtain node embedding. To capture the coupling strengths and external field strengths (i.e., edge weights $J_{i,j}$ and node weights h_i), which are crucial to determining the spin glass ground states, SGNN performs two updates at each layer, specifically, the edge-centric update and the node-centric update, respectively.

Lets $z_{(i,j)}$ denote embedding of edge (i,j) and $z_{(i)}$ embedding of node i. The edge-centric update aggregates embedding vectors from from its adjacent nodes (i.e. for edge (i,j) this update aggregate emmbedings $z_{(i)}$ and $z_{(j)}$), and then concatenates it with self-embedding $z_{(i,j)}$. Vector obtained in this way is then subject to non-linear transformation (ex. $\text{ReLU}(x) = \max(0,x)$). Mathematically it can be described by following equation

$$z_{(i,j)}^{k+1} = \text{ReLU}(\gamma_\theta(z_{(i,j)}^k) \oplus \phi_\theta(z_{(i)}^k + z_{(j)}^k)), \tag{4}$$

where $z_{(i,j)}^k$ denotes encoding of edge (i,j) obtained after k layers. Similary $z_{(i)}^k$ denotes encoding of node i obtained after k layers, γ_θ and ϕ_θ are some differentiable functions (ex. feed-foward neural networks) whih demends on set of paramethers θ. Symbol $\oplus$ is used to denote concatenation operation.

The node-centric update is defined in similar fashion. It aggregates embedding of adjacent edges, and then concatenates it with self-embedding $z_{(i)}$. Later we transform this concatenated vector to obtain final embedding. Using notation from equation 4, final result is following:

$$z_{(i)}^{k+1} = \text{ReLU}(\phi_\theta(z_{(i)}^k) \oplus \gamma_\theta(\text{E}_i^k)), \tag{5}$$

$$\text{E}_i^k = \sum_j z_{(i,j)}^k. \tag{6}$$

Edge features are initialized as edge weights $\{J_{i,j}\}$. It is not trivial to find adequate node features, as node weights $\{h_i\}$ and spins σ_i are not enough.

It is worth noting that both those operations are *message passing* schema [10]. Edge-centric update aggregate information about adjacent nodes of edge and edge itself and sends it as a "message" to this edge. Similarly, node-centric update aggregate information about edges adjacent to the node and the node itself. In those edges are also encoded information about neighbouring nodes.

We also included pooling layers not presented in the original design. We reasoned that after concatenation, vectors start becoming quite big, so we employ pooling layers to not only reduce the model size but also preserve the most essential parts of every vector.

As every node is a potential candidate for action, we call the final encoding of node i its *action embedding* and denote it as Z_i. To represent the whole Chimera (state of our environment), we use *state embedding*, denoted as Z_s, which is the sum over all node embedding vectors, which is a straightforward but empirically effective way for graph-level encoding [15].

Decoding Once all action embeddings Z_i and state embedding Z_s are computed in the encoding stage, the decoder will leverage these representations to compute approximated state-action value function $Q(s, a; \Theta)$ which predicts the expected future rewards of taking action a in state s, and following the policy π_Θ till the end. Specifically, we concatenate the embeddings of state and action and use it as decoder input. In principle, any decoder architecture may be used. Here, we use a standard feed-forward neural network. Formally, the decoding process can be written as:

$$Q(s, a^{(i)}; \Theta) = \psi_\Theta(Z_s \oplus Z_i), \tag{7}$$

where ψ_Θ is a dense feed-forward neural network.

3.3   Training

We train our model on randomly generated Chimera instances. We found that the minimal viable size of the training instance is C_3 (as a reminder, C_3 is Chimera architecture with nine unit cells arranged into a 3×3 grid, which gives us 72 spins). Smaller instances lack couplings between clusters, crucial in full Chimera, which leads to poor performance. We generate $\{J_{i,j}\}$ and $\{h_i\}$ from normal distribution $\mathcal{N}(0, 1)$ and starting spin configuration σ from uniform distribution. To introduce low-energy instances, we employed the following pre-processing procedure. For each generated instance, with probability $p = 10\%$, we perform standard simulated annealing before passing the instance through SGNN.

We seek to learn approximation of optimal action-value function $Q(a, s; \Theta)$, so as reinforcement learning algorithm we used standard n-step deep Q learning [23,20] with memory replay buffer. During episode we collect sequence of states action and rewards $\tau = (s_0, a_0, r_0, \ldots, s_{T-1}, a_{T-1}, r_{T-1}, s_T)$ with terminal state as final element. From those we construct n-step transitions $\tau_t^n = (s_t, a_t, r_{t,t+n}, s_{t+n})$ which we collect in memory replay buffer $\mathcal{B}$. Here $r_{t,t+n} = \sum_{k=0}^{k=n} \gamma^k r_{t+k}$ is return after n-steps.

3.4   Simulated Annealing with Reinforcement

Simulated annealing with reinforcement (SAwR) combines machine learning and classical optimization algorithm. Simulated annealing (SA) takes its name from

a process in metallurgy involving heating a material and then slowly lowering the temperature to decrease defects, thus minimizing the system energy. In SA, we start in some state s and in each step, we move to a randomly chosen neighboring state s'. If a move lowers energy $E(s)$ of the system, we accept it. If it doesn't, we use the so-called the Metropolis-Hasting criterion.

$$\mathbb{P}(\text{accept } s' \mid s) = \min(1, e^{-\beta \Delta E}), \tag{8}$$

where $\Delta E = E(s') - E(s)$ and β denotes inverse temperature $1/T$. In our case, the move is defined as a single-spin flip. Simulated annealing tends to accept all possible moves at high temperatures (i.e., lower β). However, it likely accepts only those moves that lower the energy at low temperatures.

Our idea is to reinforce random sampling with a trained model. It means that at low temperatures, instead of using the Metropolis-Hasting criterion, we perform a single pass of the DIRAC episode.

4   Experiments

We collected data from the D-Wave 2000Q device using default parameters (number of samplings, annealing time, etc.). We have generated 500 random instances of sizes C_4, C_8, C_{12} and C_{16}, corresponding to systems of sizes 128, 512, 1152 and 2048 spins respectively. We used identical distributions to training instances, so $\{J_{i,j}\}$ and $\{h_i\}$ was generated from normal distribution $\mathcal{N}(0,1)$ and starting spin configuration σ from uniform distribution. We then used quantum annealing to obtain the low energy states of generated instances.

We have used three methods - standard simulated annealing, a single pass of spin-flipping procedure and simulated annealing with reinforcement. Results are shown in figures 5a and 5b.

We tested for two metrics: the probability of finding lower energy states and the mean value of an improvement over starting energy state. To compute the probability for each Chimera size, we started with proposed solutions obtained from quantum annealer and tried to lower them using different tested methods. Then we counted those instances for which a lower energy state was found. We define the value of the improvement as the difference between starting energy state and the lowest energy state found by the tested method in abstract units of energy.

Simulated annealing with reinforcement achieved lower probabilities of finding a lower energy state. Although the difference between SAwR and traditional simulated annealing is slight, its consistency across all sizes suggests that it is systemic rather than random noise. The single pass of the spin-flipping procedure was the order of magnitude worse, reaching approximately 1% success rate.

It is interesting that, on average, SAwR was able to find a better low energy state than simulated annealing, but still, the difference is not significant.
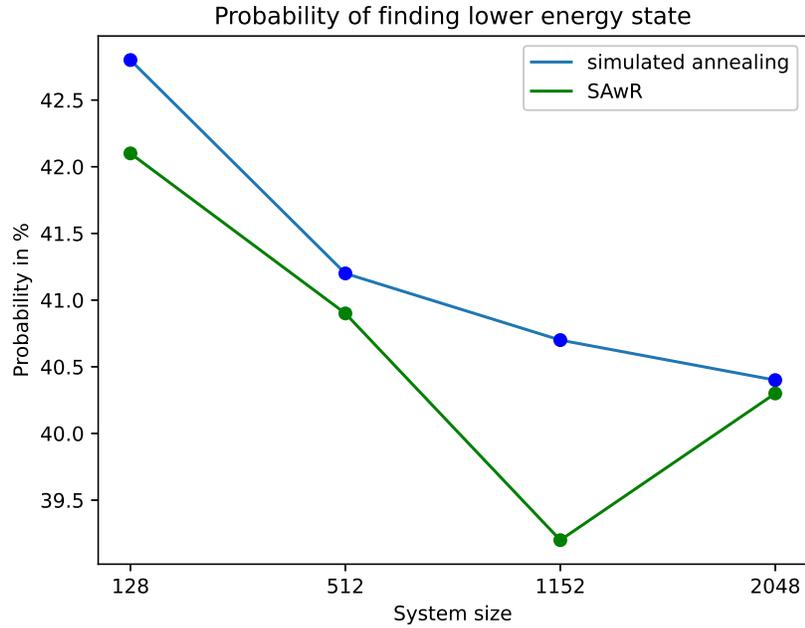
(a) The probability of finding a lower energy state was computed over 500 random instances for each Chimera size. Here we decided to omit results for a single pass of the spin flipping procedure because its results were the order of magnitude worse, making the figure hard to read.
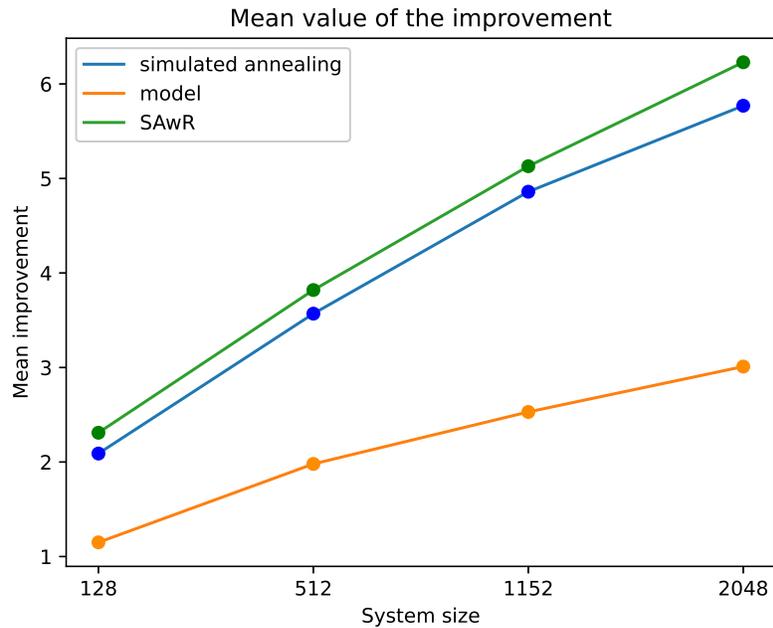
(b) Mean value of the improvement. We define the value of the improvement as the difference between starting energy state and the lowest energy state found by the tested method in abstract units of energy. The mean was computed over all instances where the method could find improvement

Fig. 5: Results of our experiments for tested metrics. By model, we define a single pass of the spin flipping procedure. SAwR denotes simulated annealing with reinforcement.

5   Discussion and Further Work

The real-life Chimera graph is a much more complex problem than the regular lattice employed in [8], which may be the reason for poor performance. However, we managed to replicate the excellent scaling of DIRAC. We trained our model on relatively small instances and employed it for large ones. We did not observe significant differences in performance relative to the size of the system. Much more work is needed because more complex architectures are deployed (Pegasus, Zephyr) by D-wave systems.

One possible avenue of research is changes in architecture. Right now goals of the encoder and decoder are quite different. The encoder tries to encode information while the decoder leverages them for reinforcement learning. Training them both at the same time might be difficult. One option is to divorce them from a single architecture. For example, we may use graph autoencoder [16,22] to train the encoder. Then for the reinforcement learning part, we would use an already trained encoder and train only the neural network responsible for approximating the action-value function.

Another option is to use different reinforcement learning algorithms. Asynchronous methods have been shown to consistently beat their synchronous counterparts, especially asynchronous advantage actor-critic [21], but asynchronous Sarsa or Q-learning also look promising. Methods based on Monte Carlo tree search inspired by AlphaZero [28] also seems promising. It has shown excellent performance on tasks involving large search space (ex. Chess, Go).

Acknowledgments

References

1. Ayanzadeh, R., Dorband, J.E., Halem, M., Finin, T.: Post-quantum error-correction for quantum annealers. Preprint at https://arxiv.org/abs/2010.00115 (2020)
2. Boothby, K., King, A.D., Raymond, J.: Zephyr Topology of D-Wave Quantum Processors. Tech. rep., D-Wave Systems Inc. (2021)

3. Bryngelson, J.D., Wolynes, P.G.: Spin glasses and the statistical mechanics of protein folding. Proceedings of the National Academy of Sciences of the United States of America **84**(21), 7524–7528 (1987). https://doi.org/10.1073/pnas.84.21.7524

4. Bunyk, P.I., et al.: Architectural considerations in the design of a superconducting quantum annealing processor. IEEE Transactions on Applied Superconductivity **24**(4), 1–10 (2014). https://doi.org/10.1109/TASC.2014.2318294

5. D-Wave Systems: The d-wave clarity roadmap (2021), https://www.dwavesys.com/media/xvjpraig/clarity-roadmap_digital_v2.pdf, visited 2022-01-26

6. D-Wave Systems: Getting Started with D-Wave Solvers (2021), visited 2022-02-15

7. Deng, Q., Averin, D.V., Amin, M.H., Smith, P.: Decoherence induced deformation of the ground state in adiabatic quantum computation. Scientific reports **3**(1), 1–6 (2013). https://doi.org/10.1038/srep01479

8. Fan, C., et al.: Finding spin glass ground states through deep reinforcement learning. Preprint at https://arxiv.org/abs/2109.14411 (2021)

9. Gilmer, J., Schoenholz, S.S., Riley, P.F., Vinyals, O., Dahl, G.E.: Neural Message Passing for Quantum Chemistry. In: Precup, D., Teh, Y.W. (eds.) Proceedings of the 34th International Conference on Machine Learning. Proceedings of Machine Learning Research, vol. 70, pp. 1263–1272. PMLR (2017)

10. Hamilton, W.L.: Graph representation learning. Synthesis Lectures on Artificial Intelligence and Machine Learning **14**(3), 1–159 (2020). https://doi.org/10.2200/S01045ED1V01Y202009AIM046

11. Jansen, S., Ruskai, M.B., Seiler, R.: Bounds for the adiabatic approximation with applications to quantum computation. Journal of Mathematical Physics **48**(10), 102111 (2007). https://doi.org/10.1063/1.2798382

12. Johnson, M., et al.: Quantum annealing with manufactured spins. Nature **473**, 194–8 (2011). https://doi.org/10.1038/nature10012

13. Kadowaki, T., Nishimori, H.: Quantum annealing in the transverse ising model. Phys. Rev. E **58**, 5355–5363 (1998). https://doi.org/10.1103/PhysRevE.58.5355

14. Kato, T.: On the adiabatic theorem of quantum mechanics. Journal of the Physical Society of Japan **5**(6), 435–439 (1950). https://doi.org/10.1143/JPSJ.5.435

15. Khalil, E., Dai, H., Zhang, Y., Dilkina, B., Song, L.: Learning Combinatorial Optimization Algorithms over Graphs. In: Guyon, I., Luxburg, U.V., Bengio, S., Wallach, H., Fergus, R., Vishwanathan, S., Garnett, R. (eds.) Advances in Neural Information Processing Systems. vol. 30. Curran Associates, Inc. (2017)

16. Kipf, T.N., Welling, M.: Variational graph auto-encoders. Preprint at https://arxiv.org/abs/1611.07308 (2016)

17. Kirkpatrick, S., Toulouse, G.: Configuration space analysis of travelling salesman problems. Journal de Physique **46**(8), 1277–1292 (1985). https://doi.org/10.1051/jphys:019850046080127700

18. Lucas, A.: Ising formulations of many np problems. Frontiers in Physics **2**, 5 (02 2014). https://doi.org/10.3389/fphy.2014.00005

19. McGeoch, C.C.: Adiabatic quantum computation and quantum annealing: Theory and practice. Synthesis Lectures on Quantum Computing **5**(2), 1–93 (2014)

20. Mnih, V., et al.: Playing atari with deep reinforcement learning. Preprint at https://arxiv.org/abs/1312.5602 (2013)

21. Mnih, V., et al.: Asynchronous methods for deep reinforcement learning. In: International conference on machine learning. pp. 1928–1937. PMLR (2016)

22. Pan, S., Hu, R., Long, G., Jiang, J., Yao, L., Zhang, C.: Adversarially regularized graph autoencoder for graph embedding. In: Proceedings of the 27th International Joint Conference on Artificial Intelligence. p. 2609–2615. AAAI Press (2018). https://doi.org/10.24963/ijcai.2018/362

23. Peng, J., Williams, R.J.: Incremental multi-step q-learning. In: Machine Learning Proceedings 1994, pp. 226–232. Elsevier (1994). https://doi.org/10.1016/B978-1-55860-335-6.50035-0

24. Pudenz, K.L., Albash, T., Lidar, D.A.: Error-corrected quantum annealing with hundreds of qubits. Nature communications **5**(1), 1–10 (2014). https://doi.org/10.1038/ncomms4243

25. Pudenz, K.L., Albash, T., Lidar, D.A.: Quantum annealing correction for random ising problems. Phys. Rev. A **91**, 042302 (Apr 2015). https://doi.org/10.1103/PhysRevA.91.042302

26. Rosenberg, G., Haghnegahdar, P., Goddard, P., Carr, P., Wu, K., De Prado, M.L.: Solving the optimal trading trajectory problem using a quantum annealer. IEEE Journal of Selected Topics in Signal Processing **10**(6), 1053–1060 (2016). https://doi.org/10.1109/JSTSP.2016.2574703

27. Santoro, G.E., Martoňák, R., Tosatti, E., Car, R.: Theory of quantum annealing of an ising spin glass. Science **295**(5564), 2427–2430 (2002). https://doi.org/10.1126/science.1068774

28. Silver, D., et al.: A general reinforcement learning algorithm that masters chess, shogi, and go through self-play. Science **362**(6419), 1140–1144 (2018). https://doi.org/10.1126/science.aar6404

29. Sutton, R.S., Barto, A.G.: Reinforcement learning: An introduction. MIT press (2018). https://doi.org/10.1007/978-1-4615-3618-5

30. Vinci, W., Albash, T., Paz-Silva, G., Hen, I., Lidar, D.A.: Quantum annealing correction with minor embedding. Phys. Rev. A **92** (2015). https://doi.org/10.1103/PhysRevA.92.042310

This figure "chimera.png" is available in "png" format from:

http://arxiv.org/ps/2203.02030v1

This figure "prob_plot.png" is available in "png" format from:

http://arxiv.org/ps/2203.02030v1